LA-UR-16-24607
Approved for public release; distribution is unlimited.

Title: Argonne Bubble Experiment Thermal Model Development II

Author(s): Buechler, Cynthia Eileen

Intended for: Report

Issued: 2016-07-01

Introduction

This report describes the continuation of the work reported in "Argonne Bubble Experiment Thermal Model Development".[1] The experiment was performed at Argonne National Laboratory (ANL) in 2014.[2] A rastered 35 MeV electron beam deposited power in a solution of uranyl sulfate, generating heat and radiolytic gas bubbles. Irradiations were performed at three beam power levels, 6, 12 and 15 kW. Solution temperatures were measured by thermocouples, and gas bubble behavior was observed.

This report will describe the Computational Fluid Dynamics (CFD) model that was developed to calculate the temperatures and gas volume fractions in the solution vessel during the irradiations. The previous report[1] described an initial analysis performed on a geometry that had not been updated to reflect the as-built solution vessel. Here, the as-built geometry is used. Monte-Carlo N-Particle (MCNP) calculations were performed on the updated geometry, and these results were used to define the power deposition profile for the CFD analyses, which were performed using Fluent, Ver. 16.2. CFD analyses were performed for the 12 and 15 kW irradiations, and further improvements to the model were incorporated, including the consideration of power deposition in nearby vessel components, gas mixture composition, and bubble size distribution. The temperature results of the CFD calculations are compared to experimental measurements.

Solution vessel geometry

The geometry used for both the MCNP and Fluent calculations corresponds to the as-built solution vessel shown in Figure 1. The model geometry consists of a rectangular prism with a curved front face and a tube in the center. The width of the earlier geometry was increased by 1.7 cm, and the depth (distance between the front face and central tube) was decreased by 1.6 cm. The geometry used for the analyses ignores the small changes in width and depth caused by transitions to the quartz windows and the curved front face. Based on the SolidWorks model, intermediate dimensions were chosen for these walls, so that the vessel could be modeled as a prismatic section. The thermocouples and stabilization plate were also omitted from the geometry, and the central tube was modeled going through the bottom of the vessel, rather than ending 0.58 cm from the bottom. The dimensions used for the as-built solution vessel model are shown in Table 1.

Table 1. Dimensions of MCNP model and SolidWorks geometry.

		Fluent/MCNP (cm)	SolidWorks (cm)
Depth (aligned with beam direction) (distance between curved front surface and back surface of box)	Min (center) Max (edges)	15.62 16.48	15.65 16.38
Width (perp to beam direction)		20.28	distance between sides of metal box: 19.05 distance between viewing windows: 21.52
Tube center location	center to back wall center to front wall	9.03 6.59	9.07 6.59
Tube outer diameter		3.81	3.81

[1] Buechler, Argonne Bubble Experiment Thermal Model Development, LA-UR-15-29280.

[2] Chemerisov et al., Experimental Results for Direct Electron Irradiation of a Uranyl Sulfate Solution: Bubble Formation and Thermal Hydraulics Studies, ANL/NE-15/19.

The liquid height was calculated using cross-sectional areas from the SolidWorks vessel geometry and the initial fill volume, which was reported to be 20 L.[2] Cross sectional areas were determined for four regions of the vessel, as shown in Table 2. The volume of the central tube and thermocouple probes (TCs) are accounted for in the cross sectional areas. The volume of the 1/8" diameter fill/drain tube, 9 cm^3, was included in the total volume calculation. An estimated length of 55 cm was used for the drain tube volume calculation. The volume of the thermocouple stabilization plate, 6.6 cm^3, was subtracted from the total liquid volume.

The temperature at the start of the experiment was 13.8°C, and the density was 1201.2 kg/m^3.[2] At this temperature, the 24.02 kg of uranyl sulfate fills the vessel to a calculated height of 63.0 cm. The steady state temperatures calculated using the thermocouple data for the 12 and 15 kW experiments were 45.2 and 50.5°C.[2] Accounting for the density decrease at these temperatures, the steady-state liquid levels for the 12 and 15 kW experiments were calculated to be 63.70 and 63.86 cm. These heights were used for the geometries in the MCNP and Fluent calculations for the 12 and 15 kW experiments, respectively.

MCNP model

The original MCNP model was provided by ANL[3]. It defines the geometry and materials for each component in the solution vessel. It also specifies an electron source, which is based on data obtained by exposing a Plexiglas sheet to the same rastered electron beam as used in the experiment. The MCNP model outputs that are used in the Fluent calculation are the 3-dimensional power distribution and the fraction of the total power deposited in each component.

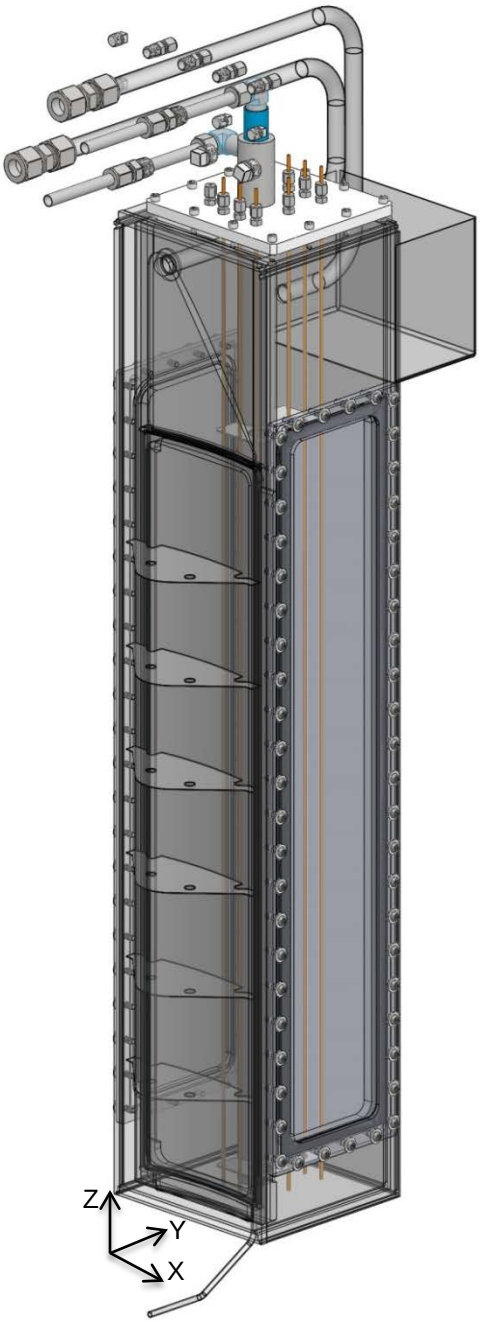

Figure 1. As-built SolidWorks model of solution vessel.

Table 2. Cross sectional areas for different vessel regions, determined from SolidWorks model.

Region	Description	Z-location (cm)	Cross sectional area (cm^2)
1	Tank bottom to bottom of TCs	0 – 0.58	295.80
2	Bottom of TCs to bottom of front window	0.58 – 3.81	283.84
3	Bottom of front window to bottom of side windows	3.81 – 9.55	292.50
4	Bottom of side windows to top of liquid	9.55 – 63.0	321.90

[3] MCNP input file, "ExpBP-DU-35MeV.i" provided by Vakhtang Makarashvili, ANL, 9/25/2015.

The MCNP model was updated to reflect the as-built geometry. The width of the liquid vessel and surrounding walls was increased by adding 0.84 cm to the X-dimension on the left and right sides. The length was decreased by subtracting 1.626 cm from the Y-dimension of the back walls. The central tube center location was also changed by decreasing the Y-dimension of its center by 1.6 cm. The height of the liquid surface was decreased by 3.84 cm for the 12 kW case and by 3.68 cm for the 15 kW case to correspond to the heights of 63.70 and 63.86 cm. Values were updated for the volumes used for calculating the fraction of beam power deposited in each component. The boundaries of the mesh tally were also changed, so that energy deposition values would be reported across the entire liquid volume. The number of requested particle histories was increased from 1e8 to 3e8 to slightly improve the accuracy of the results, and an instruction was added to save data after every 1e7 particle histories. No other changes were made to the original MCNP input file.

New power deposition results were obtained for the 12 and 15 kW cases. Power deposition values were reported (in units of kW/cm^3/kW-beam) for every cell in a 3-D grid with a spacing of 0.5 cm. This data was formatted for use in a Fluent user-defined-function (UDF) to define the volumetric heating profile. Results from MCNP calculations using 1e8 and 1e9 particle histories were compared to determine if 1e8 histories was a sufficient number. The largest difference between the two cases was 66 kW/m^3 in an area with a power deposition rate of 47000 kW/m^3, a difference of 0.14%. 1e8 was judged to be a sufficient number of particle histories. 3e8 was the number chosen for the calculations.

The list of fractional power deposited in each component was converted to total power for the 12 and 15 kW cases and is shown in Table 3 below. The power values for the highlighted components were used in the convection cooling calculations that determine the temperature profiles to be used as the boundary conditions on the cold walls of the vessel. Values for the components that are not highlighted were not used in the convection cooling calculations. These components are either not in contact with the cooling water, or the power delivered to the water from these components was judged to be insignificant.

Table 3. MCNP results for fractions and total power deposited in each component of the solution vessel.

	12 kW beam		15 kW beam	
Component	Fraction	Power, (W)	Fraction	Power, (W)
S.S-316 Vacuum flange	6.22E-04	7.46	6.21E-04	9.32
S.S-316 Window frame (vacuum to coolant)	5.30E-02	636.59	5.31E-02	795.78
S.S-316 Window frame (coolant to sample)	6.04E-02	725.30	6.04E-02	906.71
S.S-316 Wall side	2.26E-03	27.08	2.20E-03	32.94
S.S-316 Primary side	2.91E-03	34.90	2.84E-03	42.58
S.S-316 Top plate	1.64E-04	1.97	1.66E-04	2.49
S.S-316 Bottom plate	2.90E-05	0.35	2.90E-05	0.43
S.S-316 Rear wall (primary)	1.82E-02	218.41	1.73E-02	259.67
S.S-316 Bottom coolant panel	2.43E-05	0.29	2.43E-05	0.36
S.S-316 Rear coolant panel	1.36E-02	163.14	1.29E-02	194.13
Quartz window primary (wall side)	1.73E-03	20.76	1.68E-03	25.27
Quartz window primary (primary side)	2.34E-03	28.04	2.29E-03	34.42
Water coolant (edges)	4.95E-02	594.49	4.93E-02	739.30
Uranyl sulfate (130 g/L)	4.76E-01	5715.35	4.81E-01	7220.60
Al-6061 Secondary containment	9.50E-03	113.94	9.12E-03	136.83
Quartz window secondary (wall side)	4.49E-04	5.39	4.41E-04	6.62

Quartz window secondary (primary side)	5.33E-04	6.40	5.26E-04	7.89
S.S-316 Instrument plate	1.76E-04	2.11	1.78E-04	2.68
S.S-316 Central tube (outer)	4.06E-02	487.52	4.03E-02	605.14
S.S-316 Central tube (inner)	5.03E-02	603.58	4.98E-02	747.42
Water coolant (central)	6.32E-02	758.00	6.26E-02	939.32
	Total	10151.05		12709.88

The total power deposited in vessel components amounts to only about 85% of the total beam power. The remaining power escapes as bremsstrahlung photons. The power deposited in the uranyl sulfate solution is 48% of the total beam power, based on the MCNP calculation results.

CFD model

The CFD model was created using Fluent, and it was set up the same way as described in "Argonne Bubble Experiment Thermal Model Development".[1] Changes were only made to the geometry, temperature boundary conditions, and the heat and gas generation profiles. The temperature boundary conditions were recalculated based on the new heating values for the as-built geometry.

A forced convection cooling analysis was performed to determine the new linear temperature profile for each wall. A total water flow rate of 50 gpm was split between the two cooling channels according to the smallest flow area in each. Results of preliminary Fluent calculations were used to determine the power transferred from the fuel solution to the cooling water through the front, back and tube walls. Using the inlet water temperature of 19.7°C,[2] the temperature profiles on the inner surfaces of the cooled walls were calculated using the method described in the previous report.[1] One improvement was made to the method in this set of calculations, however; this was the addition of the heat loads from adjacent components in calculating the bulk water temperature rise in each channel. This includes heat deposited into the cooling water itself.

Outlet water temperatures were determined for each cooling channel based on the heat addition from the uranyl sulfate solution and the adjacent components listed in Table 3. The front and back rectangular channels were treated separately in the forced convection analysis, with the outlet temperature of the front channel used as the inlet temperature of the back channel. The following assumptions were made for components whose heat was not clearly removed by a particular cooling channel:

Table 4. Heat load assignments to the three cooling channels.

Component	Assumed fraction of heat removed by central tube	Assumed fraction of heat removed by front cooling channel	Assumed fraction of heat removed by back cooling channel
S.S-316 Vacuum flange		1	
S.S-316 Window frame (vacuum to coolant)		1	
S.S-316 Window frame (coolant to sample)		1	
S.S-316 Wall side		0.5	0.5
S.S-316 Primary side		0.5	0.5
S.S-316 Rear wall (primary)			1
S.S-316 Rear coolant panel			1
Quartz window primary (wall side)		0.5	0.5

Quartz window primary (primary side)		0.5	0.5
Water coolant (edges)		0.75	0.25
S.S-316 Central tube (outer)	1		
S.S-316 Central tube (inner)	1		
Water coolant (central)	1		

The heat deposited in the stainless steel side walls and quartz windows was assumed to be equally removed by the front and back walls, because the temperature of the liquid is quite uniform from the front of the tank to the back, and the temperature difference between the front and back walls (~2°C) is much less than the difference between the liquid and the walls (~35°C).

The volumes of water in the front and back cooling channels were not treated separately in the MCNP model. It was modeled as a single cell, Water coolant (edges), so 75% of the total power in the cell was assumed to be deposited in the front cooling channel and 25% was assumed to be deposited in the back. This assumption was based only on the knowledge that the uranyl sulfate and central tube prevent much of the electron beam from reaching the back wall, so most of the power in this cell must be removed by the front channel. The water in the central tube was also treated as a single cell, so the heat deposited in the outer channel was not separated from that in the inner channel. In the experiment, the heat deposited in the upward-flowing inner channel does not contribute to the temperature rise in the outer downward-flowing channel, but it was included in the calculation. This results in a somewhat elevated temperature definition on the central tube wall.

The fractions of the total power removed by each cooling channel were recalculated for this new geometry. Preliminary Fluent results indicated that the front, back and tube walls removed 40%, 34%, and 26% of the total power, respectively.[4] The wall temperature profiles are plotted for the 12 and 15 kW cases in Figure 2 and Figure 3 for the tube, front, back and bottom walls. The temperature of the back wall is higher than the front wall, because the stainless steel plate separating the cooling water from the solution is 2.5 times thicker than the plate in the front.

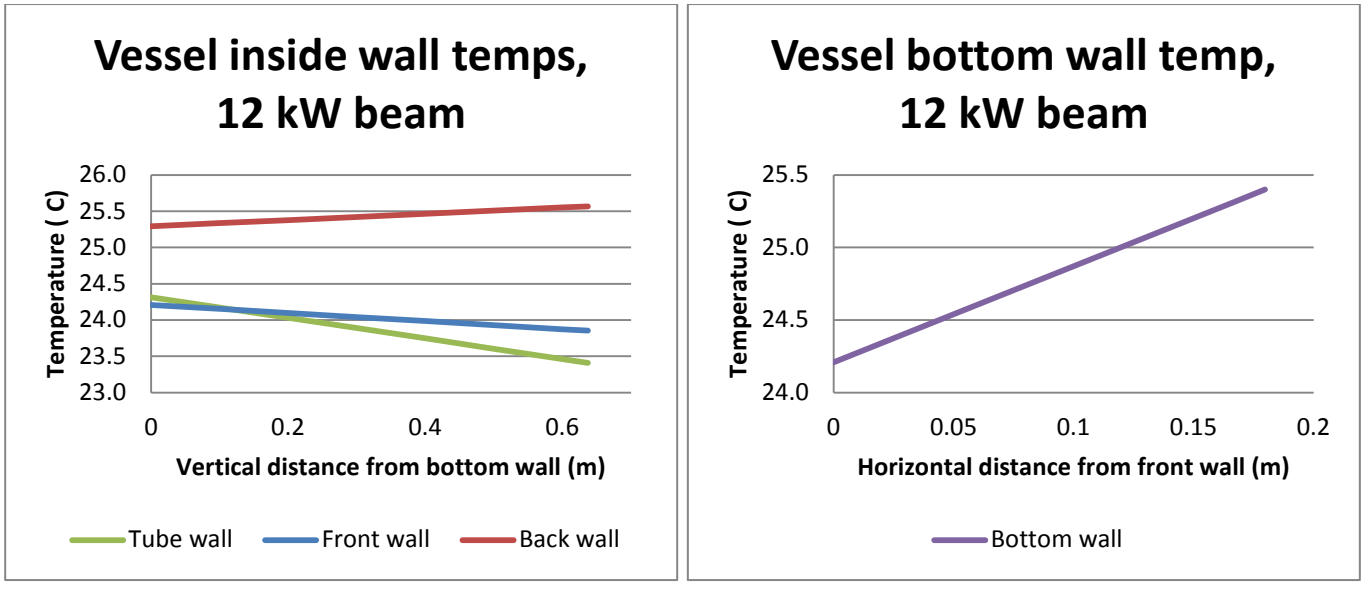

Figure 2. Cold wall temperature profiles for 12 kW case.

[4] Final results show little change from the preliminary percentages. The front, back and tube removed 40%, 35.5%, and 24.5% of the total power, respectively, for both the 12 and 15 kW cases.

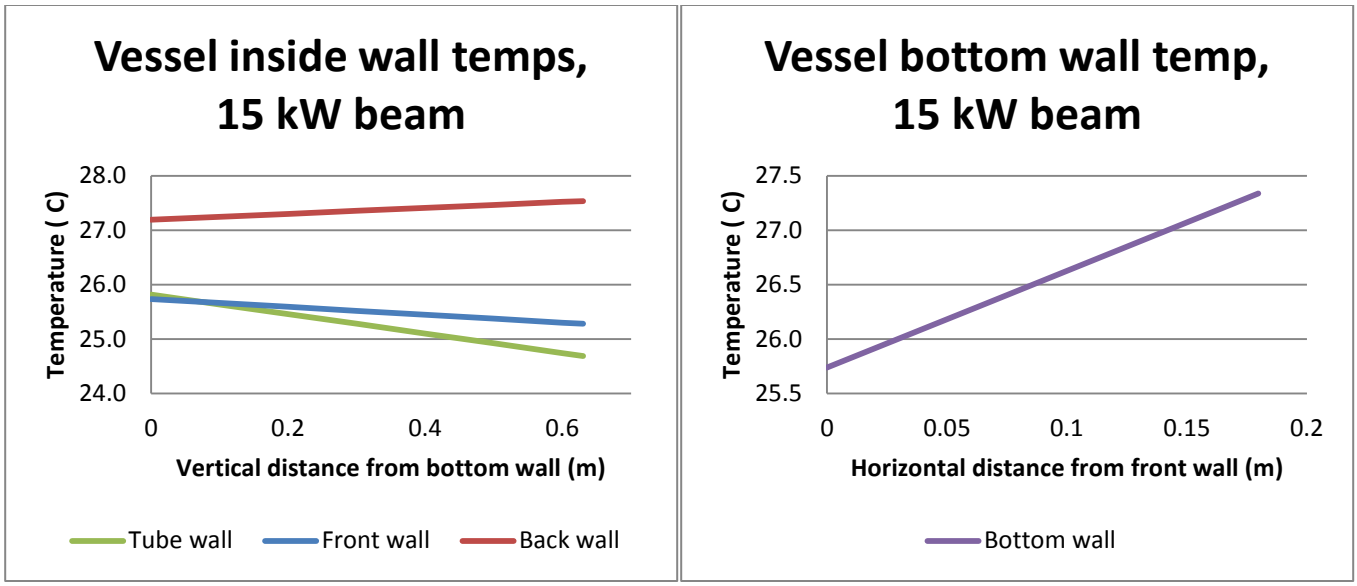

Figure 3. Cold wall temperature profiles for 15 kW case.

The volumetric heating profile was determined from the MCNP results, and the gas generation rates were estimated based on concentration measurements collected with a gas chromatograph during the irradiation.

The MCNP mesh tally grid spacing was 0.5 cm. The element edge sizing in the Fluent mesh was also approximately 0.5 cm in the bulk of the liquid volume, but the locations of the cells for the two meshes do not correspond. Each cell in the Fluent mesh was mapped to the closest cell in the MCNP mesh tally grid and assigned that value for the volumetric power deposition. The discretization of the power profile introduces some error, and the volume integral of the power profile in Fluent turns out to be 6028.77 and 7512.45 W for the 12 kW and 15 kW beam cases, respectively. These values are 5.5 and 4.0% higher than the power deposition calculated for the uranyl sulfate component by MCNP, shown in Table 3.

The power deposition profiles of the rastered electron beam are shown for the 12 kW and 15 kW cases in Figure 4. The units are W/m^3, and the electron beam is traveling in the Y-direction. The top surface of the liquid domain for the 15 kW case is 1.6 mm higher than for the 12 kW case. Figure 5 shows the power profiles for the front of the tank.

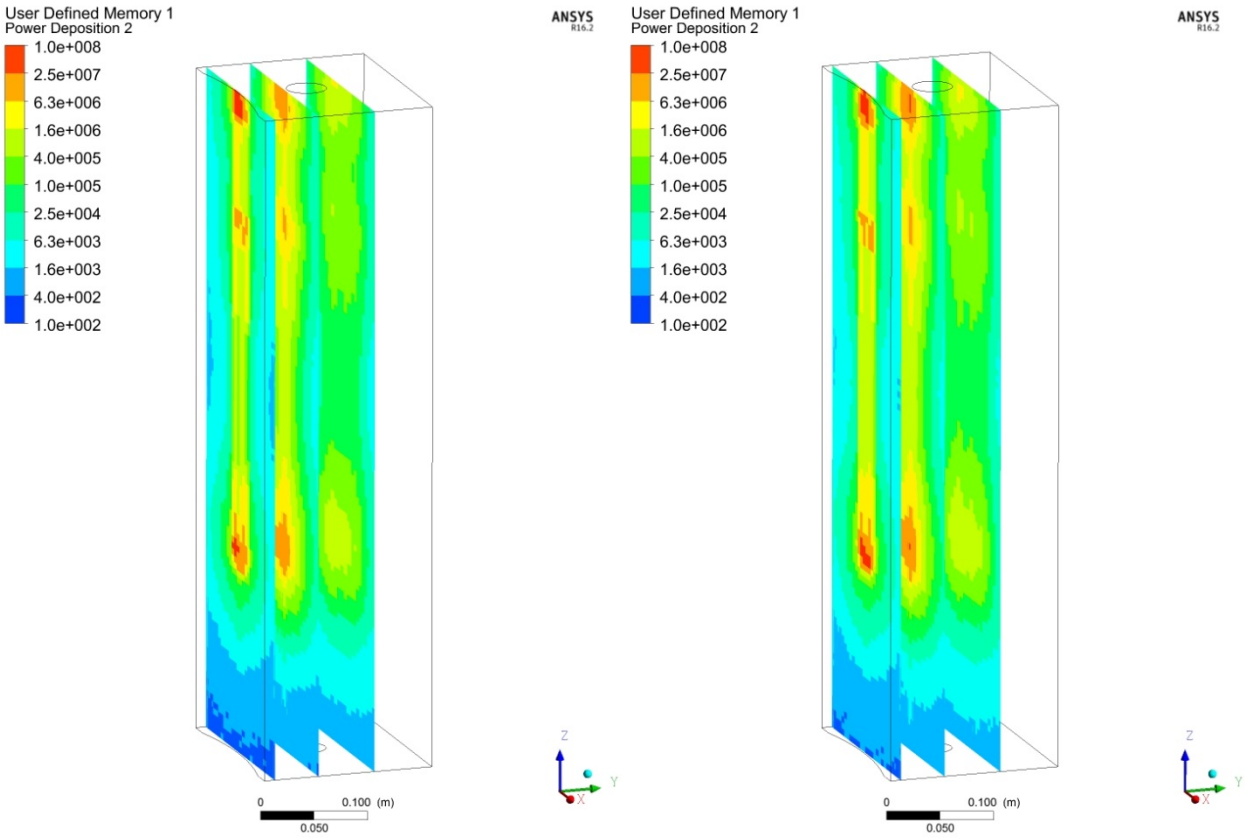

Figure 4. Power deposition profiles used as energy source definitions for 12 (left) and 15 kW (right) cases.

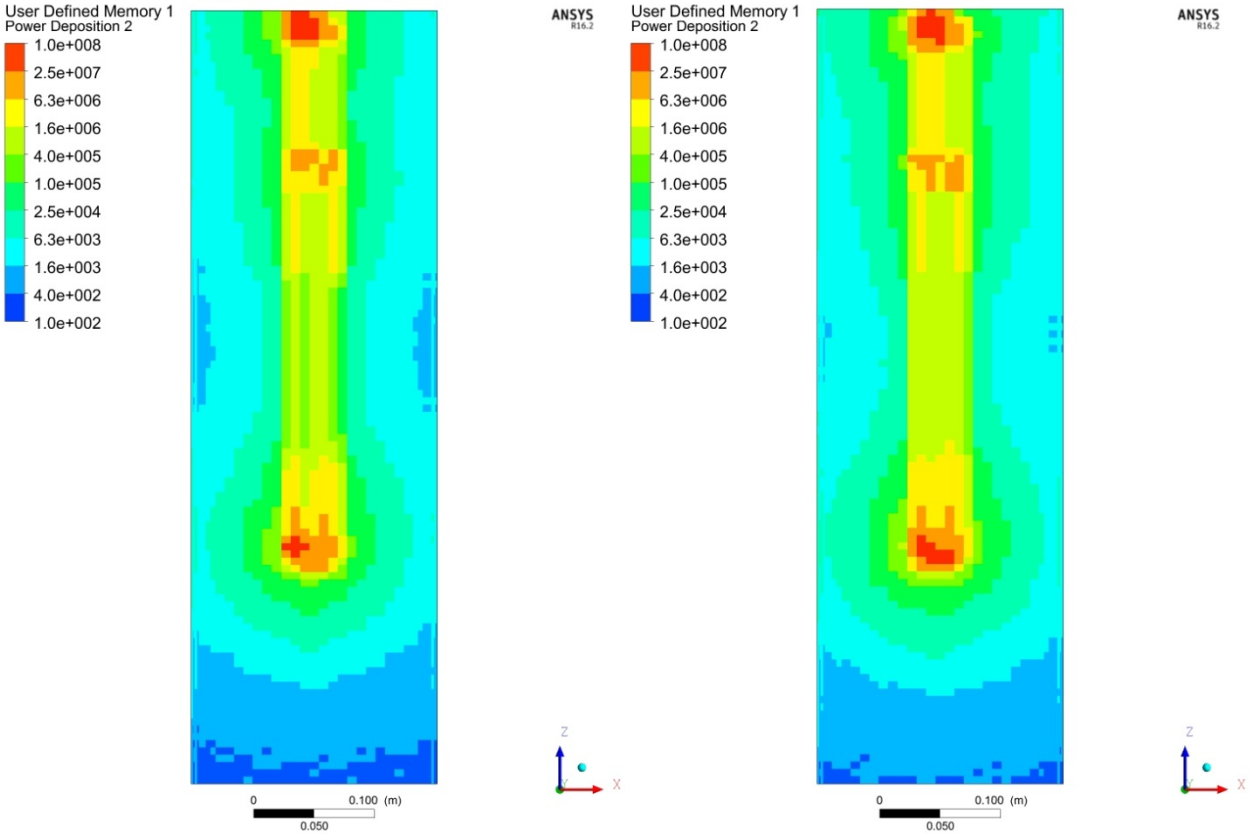

Figure 5. Power deposition profiles used as energy source definitions for 12 (left) and 15 kW (right) cases, front view.

Temperature-dependent functions for thermal conductivity and viscosity were specified for uranyl sulfate at a concentration of 135 gU/liter, and a constant specific heat of 3627.97 J/kg-K was used. The Boussinesq buoyancy approximation was used to model the natural convection. A density value of 1143 kg/m^3 and a thermal expansion coefficient of 0.00045 K^{-1} were applied to the uranyl sulfate material. These values correspond to a uranyl sulfate temperature of 50°C.

Throughout the Argonne Bubble Experiment, the percent concentrations of hydrogen and oxygen present in the helium sweep gas were measured using a gas chromatograph.[2] The chromatograph was located downstream of a 2-liter condenser to remove water vapor. Gas generation rates were calculated by converting the percent concentration values to µmoles of gas swept through the chromatograph between sampling times (~ 11 minutes).

Just before the start of the 15 kW irradiation, (250 min from start of beam), the estimated hydrogen and oxygen production rates from the 12 kW irradiation reached their peak.[2] These rates were 3.61 and 0.31 µmoles/min. Using molecular mass values[5] for H_2 and O_2 of 2.016 and 31.999 g/mol, and individual gas constants[5] of 4.1243 and 0.2598 kJ/kg-K, the mass generation rates for H_2 and O_2 were calculated using the ideal gas model[6] to be 1.19e-10 and 1.63e-10 kg/s. Combined, this gives a total mass generation rate of 2.87e-10 kg/s. This was the value used in the 12 kW Fluent calculation.

The highest hydrogen production rate attributable to the 15 kW irradiation was measured at 397 min to be 7.24 µmoles/min, and the oxygen production rate at this time was 0.70 µmoles/min. These rates combine to give a total mass generation rate of 6.1e-10 kg/s, which was used for the 15 kW Fluent calculation.

If the experiment had been allowed to reach a steady-state rate of radiolytic gas production, a stoichiometric mixture of hydrogen and oxygen would be expected. A stoichiometric mixture would be 11% H_2 and 89% O_2 by mass, but the gas mixture during the 12 kW run was calculated to be 42% H_2 and 58% O_2. Temperature-dependent material properties for this specific mixture were calculated and specified in the Fluent model. The mixture gas constant was used to determine the density function. The specific heat, thermal conductivity, and viscosity were determined at various temperatures by combining the properties of the individual gases according to mass fraction, and linear functions of temperature were fit to these values. The same properties were used for the 15 kW case, even though the gas mixture at this point in the experiment was about 40% H_2 and 60% O_2. A uniform bubble diameter of 267 µm was specified, matching the average bubble diameter measured during the experiment.[2]

The power profile values were scaled in the UDF and specified as a mass source. The volume integral of this source of gas was 2.85e-10 kg/s for the 12 kW case and 6.08e-10 kg/s for the 15 kW case.

The Green-Gauss Node Based method was used for the gradient discretization, and the QUICK method was used for discretization of all of the other flow variables. The calculation was run in steady-state (Pseudo Transient) mode and used the default under-relaxation factors. A time scale factor of 0.04 was used, which results in a pseudo-timestep value of 6.7 ms. Calculations are considered converged when the integrated surface heat flux matches the total heat generation to within 0.5% or smaller.

[5] Sonntag et al., Fundamentals of Thermodynamics, 5th Ed., 1998, Wiley.

[6] For a temperature of 45°C, the reported volume-averaged steady-state solution temperature for an electron beam power of 12 kW.

Calculation results

The steady-state calculation results for the 12 and 15 kW beam cases are presented in Table 5.

Table 5. Fluent calculation results for 12 and 15 kW.

Beam power	Max Fuel Temp (°C)	VolAve Fuel Temp (°C)	Min Z-Veloc Fuel (cm/s)	Max Z-Veloc Fuel (cm/s)	Max Vertical Veloc Bubbles (cm/s)	VolAve Vert Veloc Bubbles (cm/s)	Max Vol Frac Bubbles	VolAvg Vol Frac Bubbles
12 kW	119.0	52.5	-4.95	5.22	8.33	2.89	2.1e-3	1.3e-6
15 kW	130.9	58.7	-5.47	6.27	9.59	3.09	6.5e-3	3.5e-6

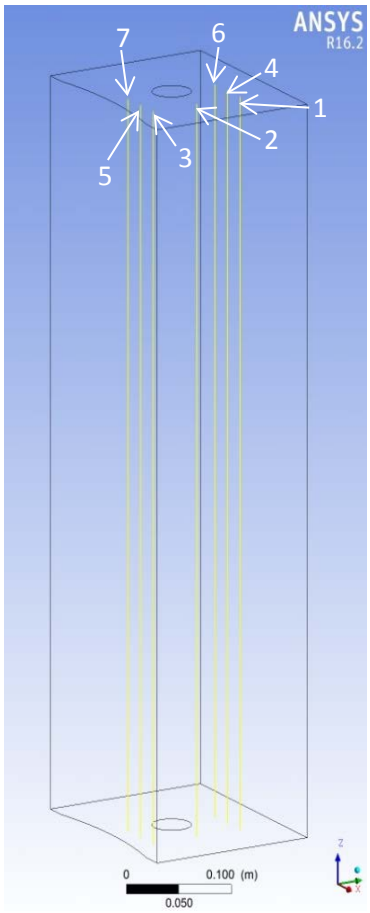

Figure 6. TC probe locations.

The temperature results at the top of the tank are above boiling for both cases. The maximum temperature measured for the 12 kW irradiation (ignoring the thermocouples directly heated by the beam) was 65.6°C, and the volume-average temperature calculated from the thermocouples was reported to be 45.2 ±0.1°C.[2] The maximum temperature measured for the 15 kW case was 71.0°C, and although no volume-average temperature was reported for the 15 kW case, the temperature calculated from the thermocouples was plotted, and it appears to be 50.5 ±0.1°C.[2] The difference between the volume-average temperature result from the simulation and the temperature calculated from experimental measurements is 7.3 and 8.2°C for the 12 kW and 15 kW cases, respectively.

Seven thermocouple probes measured temperatures at six vertical locations in the vessel during the 12 and 15 kW experiments. Their locations are shown in Figure 6. The top location for each of the seven probes was above the liquid level, so only five measurements for each probe are compared to the calculated results. Also, TCs 5 and 7 were directly heated by the beam during the experiment, so their readings are not to be considered valid measurements of the liquid temperature. The measurements from TCs 5 and 7 will not be shown with the other experimental results, but calculated temperatures at the locations of TC 5 and TC 7 will be presented.

Plots of the temperatures measured by thermocouples during the 12 and 15 kW experiments are compared to the calculated temperatures along the same vertical axes in Figure 7 and Figure 8. The calculated temperature profiles for TCs 1 - 6 are almost identical and are difficult to differentiate in the plot. The temperatures calculated for the front location, TC7, have slightly steeper increases at the bottom and top of the tank, but the variations in temperature with x and y position are very small, and in both experiment and calculation the tank temperature is mostly uniform at any given height.

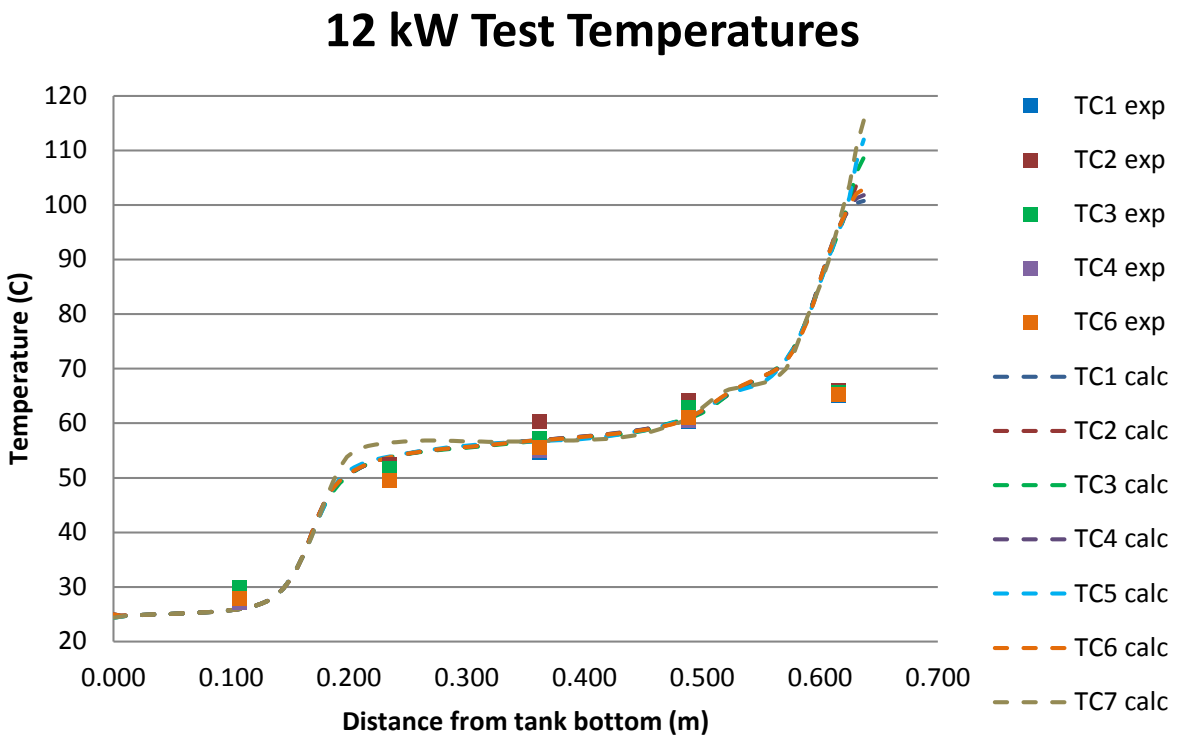

Figure 7. Experimentally-measured (square markers) and calculated (dashed lines) temperatures for the 12 kW beam test.

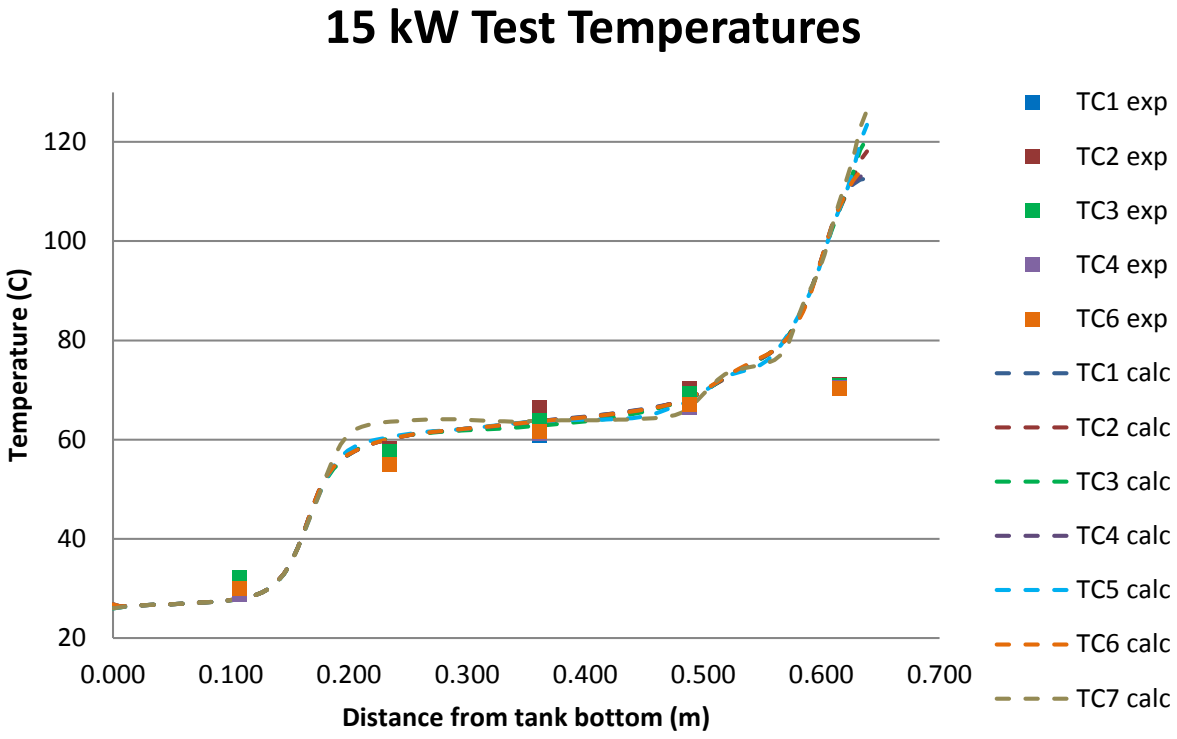

Figure 8. Experimentally-measured (square markers) and calculated (dashed lines) temperatures for the 15 kW beam test.

For all of the Fluent results figures shown, the variable data is interpolated from mesh vertex values. Temperature results are shown for the 12 and 15 kW cases in Figure 9, and bubble volume fraction results are shown in Figure 10.

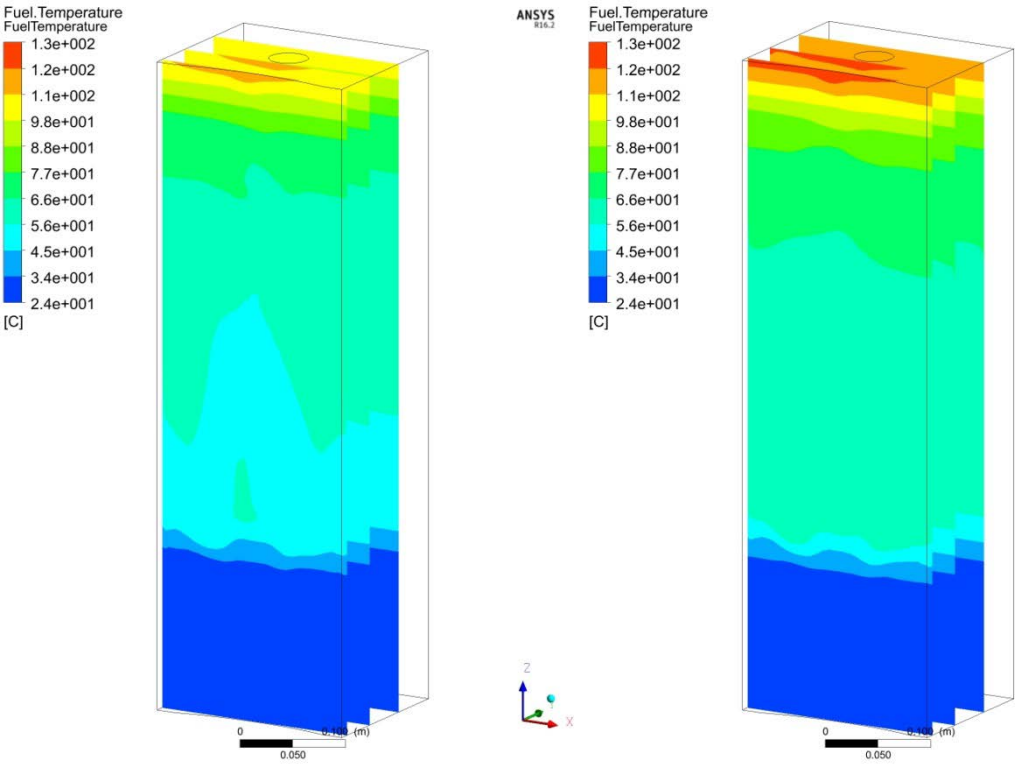

Figure 9 Steady-state liquid temperature for 12 kW (left) and 15 kW (right) cases.

During the experiment, more bubbles were observed in the front half of the domain (beam side), and bubbles started to appear at 1/3 of the height of the chamber[2]. A composite image of the bubbles in the upper, middle, and lower portions of the vessel, has been taken from the ANL report[2] and is displayed in Figure 11. The regions of higher bubble concentration are the same as those in the calculation results.

No gas volume fraction estimates were made based on experimental observations, but judging from the bubble pictures and videos, the volume fraction seems to be much higher than the calculated result of 1e-5.

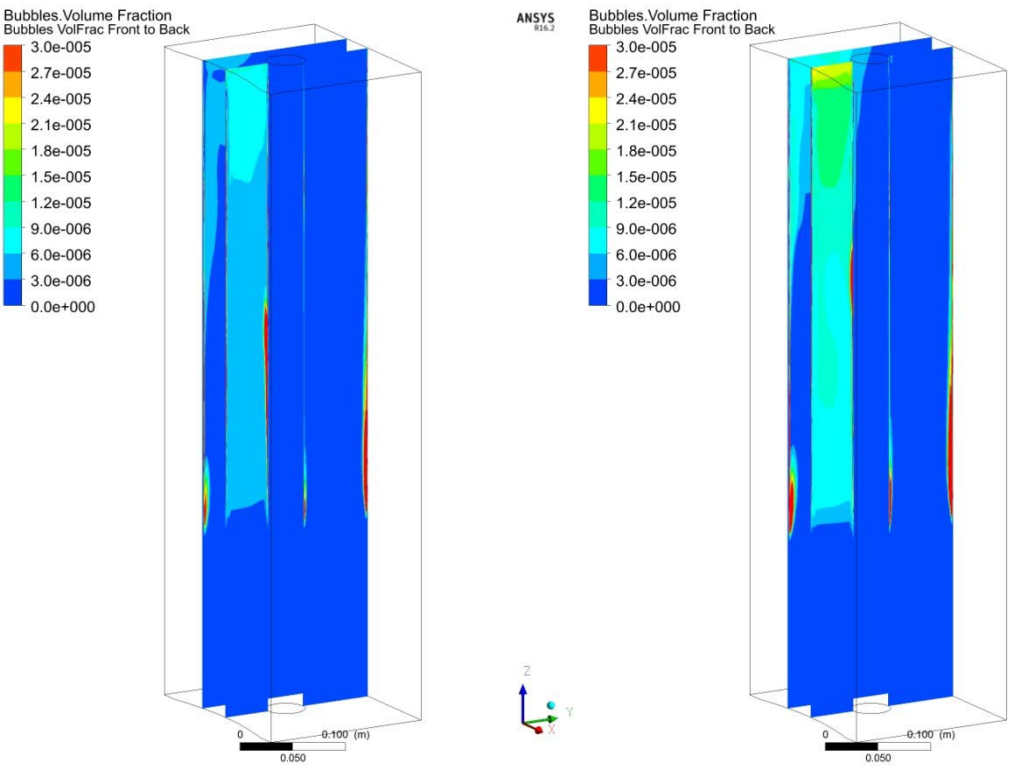

Figure 10. Volume fraction profile results for 12 kW (left) and 15 kW (right) cases.

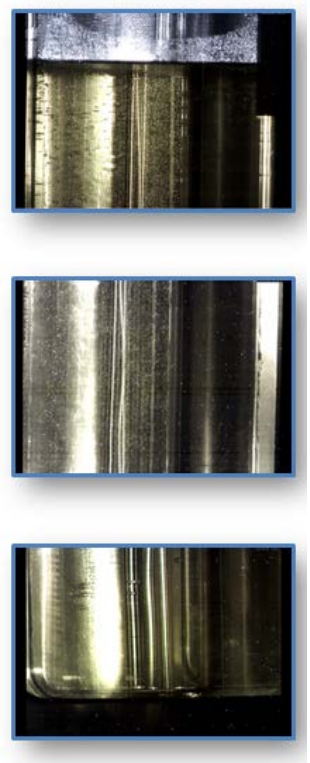

Figure 11. Image from ANL report[2] of bubbles during 12 kW run.

The liquid vertical velocity profiles are shown in Figure 12. The fuel velocity directions and magnitudes also roughly match those observed in the experiment: 1-2 cm/s near the front and top of the tank, and approximately -3 cm/s at the rear of the central tube near the mid-height[2]. The downward velocity of liquid near the cold walls creates the regions of high bubble volume fraction seen in Figure 10.

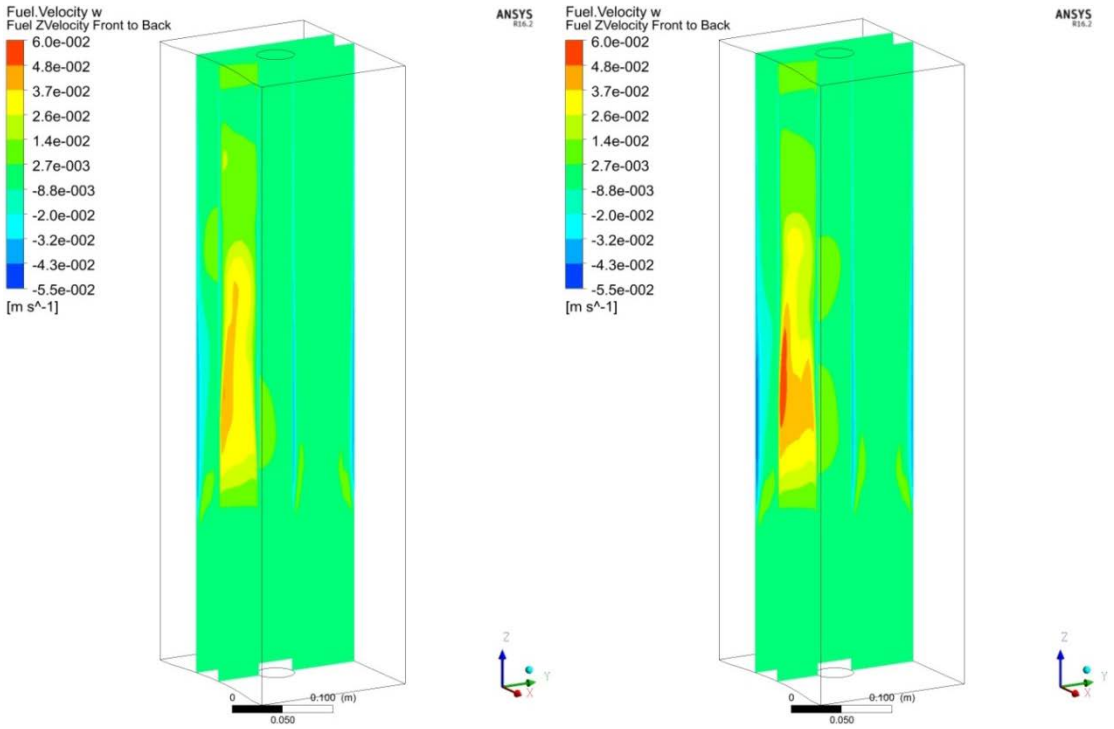

Figure 12. Liquid vertical velocity profiles for results for 12 kW (left) and 15 kW (right) cases.

The bubble vertical velocity profiles are shown in Figure 13. The calculated vertical bubble velocity near the top of the tank was 4-5 cm/s, which matches the measured vertical bubble velocity in that region.[2]

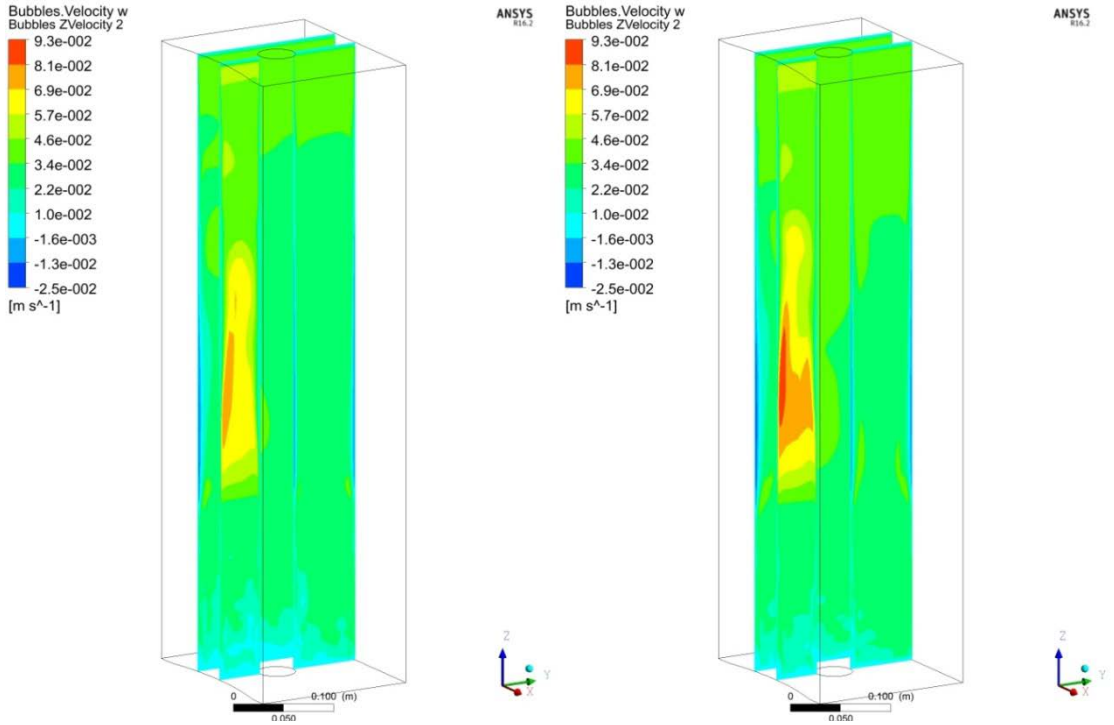

Figure 13. Bubble vertical velocity profiles results for 12 kW (left) and 15 kW (right) cases.

The average bubble velocity may be checked with the terminal velocity predicted by the force balance equation for a gas sphere of radius r moving through at liquid at constant velocity, V_0:

$$\frac{4}{3}\pi r^3 \rho_l g = \frac{4}{3}\pi r^3 \rho_g g + C_D \frac{1}{2}\rho_l {V_0}^2 \pi r^2$$

where ρ_l and ρ_g are the density of the liquid and the gas, and C_D is the drag coefficient for the sphere. This equation can be rearranged to solve for the bubble's terminal velocity:

$$V_0 = \sqrt{\frac{8rg(\rho_l - \rho_g)}{3C_D\rho_l}}$$

The particle Reynolds number[7] may be calculated by $Re_p = \frac{V_0 d}{\nu}$, where V_0 is the bubble velocity relative to the liquid, d is the bubble diameter, and ν is the kinematic viscosity of the liquid. Using the measured velocity of the bubbles of 4 cm/s, a diameter of 267 µm, a density of 1143 kg/m^3, and a dynamic viscosity of 0.000546 Pa*s, [8] the particle Reynolds number is calculated to be 22.4. This value corresponds to flow somewhere between the Stokes flow and Newtonian flow regimes for a sphere. The approximate drag coefficient, C_D, in this intermediate regime may be expressed as[9]:

$$C_D \cong \frac{18.5}{{Re_p}^{3/5}}$$

This gives a drag coefficient of 2.87. Using a gas density at 50°C of 0.166 kg/m^3, the terminal velocity is evaluated to be 3.5 cm/s, which is close to the measured velocity. The variations in bubble velocity are due to the addition of the liquid velocity in the region to the terminal bubble velocity, as can be seen in Figure 12 and Figure 13.

Model variations

Several variations of the Fluent model for the 12 kW beam case were studied to compare with the results of the baseline model described in the previous section. The first variation made use of a temperature-dependent liquid density to model the buoyancy-driven flow instead of the Boussinesq buoyancy approximation. The results of the two models were not significantly different, as can be seen in Table 6. The maximum fuel temperature was slightly lower for the temperature-dependent density case, but the temperature profiles in the vertical direction were essentially the same.

Table 6. Calculation results for variations in baseline model.

12 kW Model	Max Fuel Temp (°C)	VolAve Fuel Temp (°C)	Min Z-Veloc Fuel (cm/s)	Max Z-Veloc Fuel (cm/s)	Max Vertical Veloc Bubbles (cm/s)	VolAve Vert Veloc Bubbles (cm/s)	Max Vol Frac Bubbles	VolAvg Vol Frac Bubbles
Baseline	119.0	52.5	-4.95	5.22	8.33	2.89	2.1e-3	1.3e-6
Temp-dept density	112.7	52.2	-5.05	5.59	8.69	2.88	2.3e-3	1.3e-6
Population balance	118.8	52.6	-4.93	5.46	9.29	2.60	4.0e-3	1.4e-6

[7] Street et al., Elementary Fluid Mechanics, 7th Ed, p. 501.
[8] These values correspond to a uranyl sulfate temperature of 50°C.
[9] Bird, Transport Phenomena, p. 194.

The next variation was performed using a population balance model for the bubble sizes instead of a single size of 267 µm, as is used in the baseline model. Bubble sizes were measured during the experiment, and a distribution of sizes was determined for the 12 kW case at a location near the top of the liquid and just inside the center channel.[2] The size distribution is centered at 267 µm and ranges from 100 µm to 440 µm. A discrete phase population balance model was created using three bubble sizes: 134 µm, 267 µm, and 400 µm. Bubbles of 267 µm appear about three times as frequently as 134 and 400 µm bubbles, based on the measured size distribution. The radiolytic gas is introduced to the liquid as a mass source, and the mass source fraction was defined for each size so that the steady-state number fractions of the bubbles roughly corresponded to the measured distribution. The settings and number fraction results are shown in Table 7.

Table 7. Bubble sizes, fraction of mass introduced at each size, and resulting number fraction to compare to experiment

Bubble size (µm)	mass source fraction	steady-state number density (particles/m^3)	steady-state number fractions
134	0.000002	21,000	0.2
267	0.019998	62,000	0.6
400	0.980000	20,000	0.2

Bubble sizes are fixed throughout the calculation; they do not expand, break, or coalesce. While 98% of the mass of the radiolytic gas is introduced as 400 µm bubbles, only about 20% of the total number of bubbles in the vessel is comprised of 400 µm bubbles. Results are not altered significantly by the addition of the two other bubble sizes, as shown in Table 6. Total bubble volume fraction increased slightly, but the temperature distribution was not affected.

The temperature profiles in the vertical direction for both the temperature-dependent density model and the population balance model were indistinguishable from the calculated temperature profiles shown in Figure 7.

Gas generation sensitivity analysis

A calculation for the 12 kW beam case was performed in which the gas generation was turned off completely, and no change in the temperature distribution was noticed. This result is in contrast to the result of bubble introduction in similar systems, where bubbles have been shown to have a significant effect on heat transfer and the liquid temperature profile.[10,11]

Large quantities of bubbles were reported to have been seen in all of the irradiations[2], so ignoring the gas generation rates calculated from the gas chromatograph measurements, several calculations were performed for the 12 kW beam case using increased gas generation rates. Three cases were evaluated, with gas generation rates defined to be 100, 1,000, and 10,000 times the rates measured in the experiment. Table 8 compares the results of the baseline calculation to those with the increased gas generation rates. The last column lists the level height increase that would be expected due to the bubble volume. The uncertainty in the measurement of the solution height change is reported to be ± 0.20 mm,[2] so the level height increase due to bubble volume would have been undetectable for all but the last case, with a gas generation rate four orders of magnitude higher than what was measured.

The average power density in the solution at 12 kW is 302 kW/m^3, or 0.302 kW/liter. This is about 15% of the power density at which the homogeneous uranyl-nitrate solution reactor, SUPO, operated, but the gas generation rate, adjusted for power, is orders of magnitude lower than was measured for SUPO.[12] The total radiolytic gas mass

[10] Bull, Effects of Gas Bubble Production on Heat Transfer from a Volumetrically Heated Liquid Pool, Ph.D Thesis, 2014.
[11] Buechler, Aqueous Solution Vessel Thermal Model Development, LA-UR-15-23537.
[12] Bunker, Status Report on the Water Boiler Reactor, LA-2854, 1963.

generation rate measured during operation of SUPO was 2.78e-9 kg/s/W. At this rate, the mass generation rate that would be expected during the 12 kW irradiation would be about 1.6e-5 kg/s. The total mass generation rate calculated for the 12 kW bubble experiment, based on the measured hydrogen and oxygen concentrations in the downstream sweep gas, was 2.87e-10 kg/s.

The electrolysis mechanism for SUPO was fission, whereas the mechanism for the bubble experiment was electron beam irradiation, but if deposited power is the sole consideration, the mass generation rate measured in the bubble experiment is five orders of magnitude low.

Table 8. Results for calculations using 1X, 100X, 1000X, and 10000X the measured gas generation rate.

Gas generation rate (kg/s)	Max Fuel Temp (°C)	VolAve Fuel Temp (°C)	Min Z-Veloc Fuel (cm/s)	Max Z-Veloc Fuel (cm/s)	Max Vertical Veloc Bubbles (cm/s)	VolAve Vert Veloc Bubbles (cm/s)	Max Vol Frac Bubbles	VolAvg Vol Frac Bubbles	Level height increase due to bubbles (mm)
2.85e-10 (Baseline)	119.0	52.5	-4.95	5.22	8.33	2.89	2.1e-3	1.3e-6	0.001
2.85e-8	117.4	53.1	-4.91	5.32	8.42	2.95	9.2e-3	7.3e-5	0.046
2.85e-7	70.3	52.7	-7.44	10.6	13.8	2.94	1.7e-2	3.9e-4	0.243
2.85e-6	54.1	45.0	-16.8	27.8	30.7	2.71	8.0e-2	4.6e-3	2.872

Figure 14 compares the vertical temperature profiles of the calculations performed for the four different gas generation rates. Higher bubble concentrations result in a more homogeneous temperature profile. In all of the cases, there is little temperature difference between the different TC locations for a given height. The calculation using a 1000X gas generation rate results in a temperature profile that is very similar to the measured temperatures.

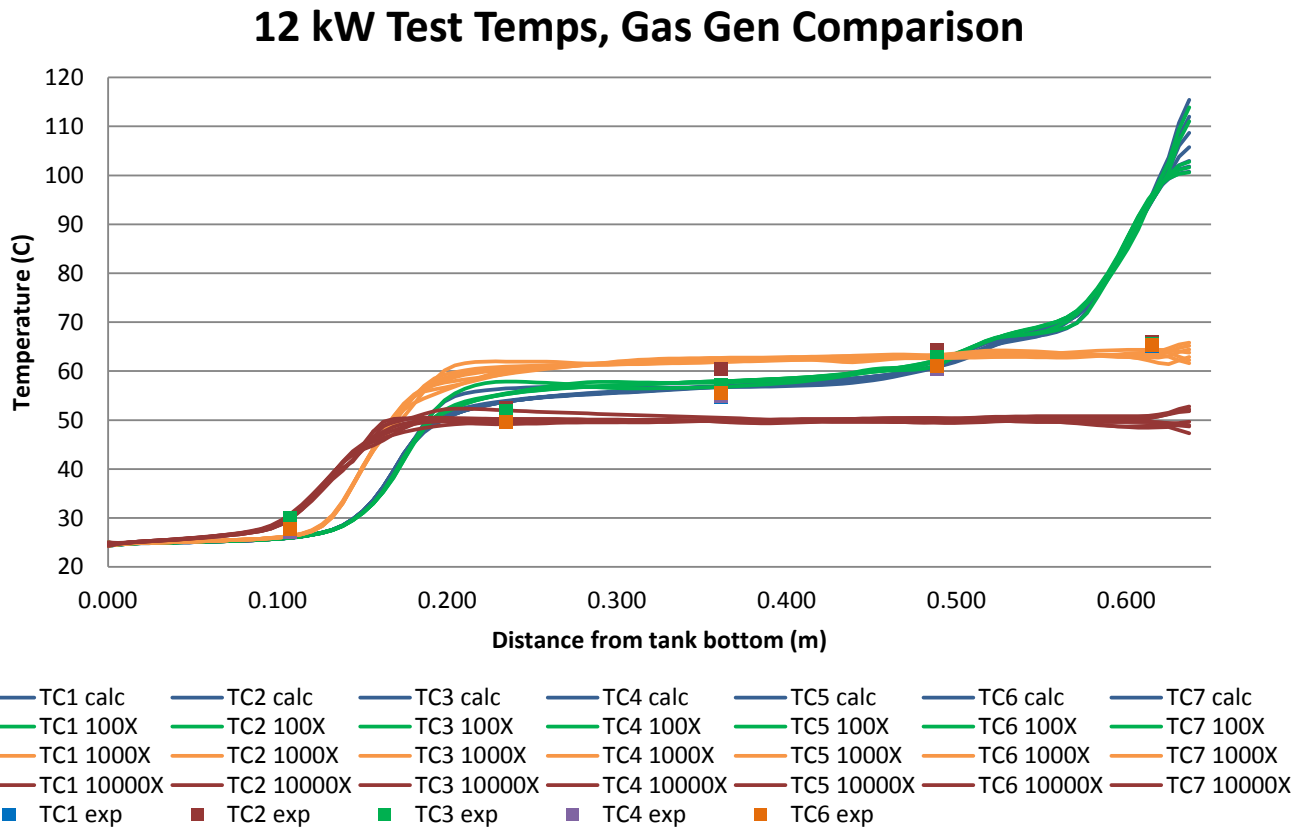

Figure 14. Temperature profiles for gas generation rates of 1X (blue), 100X (green), 1000X (orange), and 10000X (red) the measured values.

Conclusion

Calculated temperatures match measurements fairly well in the central portion of the tank but depart from measured temperatures drastically near the top. The temperatures calculated for the upper portion of the tank are believed to be high because of the difference between the actual gas generation rate and the rate that was inferred from measurements during the experiment. Other sources of error exist but are not believed to be the major cause of the discrepancy between measured and calculated temperatures. Below is a list of possible improvements to the model and experiment.

- Model improvements
  - The accuracy of the heating profile generated by MCNP could be improved by dividing the uranyl sulfate volume into segments in the x, y and z directions. This would allow the specification of density variations throughout the liquid.
  - Certain components in the MCNP model, including cooling water volumes, could be divided up to more accurately estimate the power deposited in each component and cooling channel section.
  - The thermocouple probes could be included in the MCNP and Fluent models to determine the power deposition in these volumes and the effect of the probes on the flow.
- Experimental measurement improvements
  - A reliable measurement of the gas generation rate is the most important improvement for the validation experiment. The system should be allowed to reach a steady-state gas generation condition, but if this is not possible, an accurate instantaneous gas generation rate must be measured.
  - The accuracy of the power deposition profile used as the energy source definition is dependent on the accuracy of the beam intensity measurement using the Plexiglas sheet and the vertical alignment of this scanned profile. The starting and operating liquid level height should be measured, and the position of the power profile with respect to these heights should be determined.
  - Individual water flow rate measurements could be made for the two cooling channels to improve the results of the forced convection calculations used to specify the cold wall temperatures.
  - The walls on the sides of the vessel were specified to have zero heat flux, but more accurate boundary conditions could be specified if the outside temperatures on the metal edges of the side walls were measured during the irradiations.

The CFD model does not fully capture every detail of the experiment, but it is a useful tool to make predictions. Sensitivity analyses can also help guide future tests, revealing the important parameters and indicating the measurements necessary for a useful validation experiment. With improvements to the model and some additional measurements from another bubble experiment, a more conclusive model validation could be performed.

The author gratefully acknowledges the help of Greg Dale with the MCNP calculations and interpretation of results.